Rapid Communications

In-plane magnetic penetration depth of superconducting $CaKFe_4As_4$

Rustem Khasanov,[1,*] William R. Meier,[2,3] Yun Wu,[2,3] Daixiang Mou,[2,3] Sergey L. Bud'ko,[2,3] Ilya Eremin,[4,5] Hubertus Luetkens,[1] Adam Kaminski,[2,3] Paul C. Canfield,[2,3] and Alex Amato[1]

[1]*Laboratory for Muon Spin Spectroscopy, Paul Scherrer Institut, CH-5232 Villigen PSI, Switzerland*

[2]*Division of Materials Science and Engineering, Ames Laboratory, Ames, Iowa 50011, USA*

[3]*Department of Physics and Astronomy, Iowa State University, Ames, Iowa 50011, USA*

[4]*Institut für Theoretische Physik III, Ruhr-Universität Bochum, 44801 Bochum, Germany*

[5]*Institute of Physics, Kazan Federal University, Kazan 420008, Russian Federation*

(Received 19 December 2017; revised manuscript received 8 March 2018; published 9 April 2018)

The temperature dependence of the in-plane magnetic penetration depth (λ_{ab}) in an extensively characterized sample of superconducting $CaKFe_4As_4$ ($T_c \simeq 35$ K) was investigated using muon-spin rotation (μSR). A comparison of $\lambda_{ab}^{-2}(T)$ measured by μSR with the one inferred from angle-resolved photoemission spectroscopy (ARPES) data confirms the presence of multiple gaps at the Fermi level. An agreement between μSR and ARPES requires the presence of additional bands, which are not resolved by ARPES experiments. These bands are characterized by small superconducting gaps with an average zero-temperature value of $\Delta_0 = 2.4(2)$ meV. Our data suggest that in $CaKFe_4As_4$ the $s^{\pm}$ order parameter symmetry acquires a more sophisticated form by allowing a sign change not only between electron and hole pockets, but also within pockets of similar type.

DOI: 10.1103/PhysRevB.97.140503

Since their discovery, iron-based superconductors (Fe-SCs) have attracted much interest. This broad class of materials exhibits unconventional superconducting properties due to the strong interplay of superconductivity with various electronic ground states, including a nematic phase and spin-density wave magnetism [1–5]. Recently a new Fe-SC family was synthesized, namely, $AeAFe_4As_4$ (Ae = Ca, Sr, Eu, and A = K,Rb,Cs) with superconducting transition temperature (T_c) reaching $\simeq$36 K [6,7]. $CaKFe_4As_4$ (CaK1144) is currently the most studied representative of the $AeA1144$ Fe-SC family with $T_c \simeq 35$ K and an estimated upper critical field of $H_{c2}^{\perp c} \simeq 92$ T [6,7]. High-resolution angular-resolved photoemission (ARPES), nuclear magnetic resonance, tunneling, penetration depth measurements [8–12], as well as density functional theory (DFT) calculations [8,13] support multiband superconductivity in $CaKFe_4As_4$ with Cooper pairing occurring in electron- and hole-like bands.

Despite the good agreement between results obtained by different techniques, the gap structure as well as the gap magnitudes are still not conclusively determined. DFT calculations suggest that ten bands cross the Fermi level (six hole- and four electron-like bands) [8,13]. ARPES experiments, on the other hand, reveal only the presence of four bands (α, β, γ, and δ bands) with nearly isotropic superconducting energy gaps with the corresponding zero-temperature values of $\Delta_{0,\alpha} = 10.5$, $\Delta_{0,\beta} = 13$, $\Delta_{0,\delta} = 8$, and $\Delta_{0,\gamma} = 12$ meV [8]. Tunneling experiments show that the superconducting gaps are spread between 1 and 10 meV with a broad peak appearing at around 3 meV, whereas the superfluid density measurements suggest nodeless two-gap superconductivity with a larger gap of ∼6–10 meV and a smaller gap of ∼1–4 meV [9,10,12].

In this Rapid Communication, we report on measurements of the in-plane magnetic penetration depth (λ_{ab}) and the vortex core size (ξ_{ab}) in a $CaKFe_4As_4$ single-crystal sample by means of the muon-spin rotation (μSR) technique. The obtained temperature dependence of λ_{ab} was compared with the calculations based on the analysis of the electronic band structure and the momentum-dependent superconducting gap extracted from the ARPES data. An agreement between the results obtained by both techniques requires the presence of additional bands which were not resolved in ARPES experiments.

$CaKFe_4As_4$ single crystals were grown from a high-temperature Fe-As rich melt and extensively characterized via thermodynamic and transport measurements [7]. A fraction of the ARPES data was previously reported in Ref. [8]. A crystal with dimensions of $\simeq 4.0 \times 4.0 \times 0.1$ mm^3 was used for the μSR experiments, which were carried out at the πM3 beam line using the GPS spectrometer (Paul Scherrer Institut, Switzerland) [14]. Transverse-field (TF) μSR measurements were performed at temperatures from $\simeq$1.5 to 50 K. The external magnetic field (H_{ap}) ranging from 5 to 580 mT was applied along the crystallographic c axis of the crystal. A spin rotator was used to orient the initial spin polarization of the muon beam at 45° with respect to the applied field. A special sample holder designed to measure thin samples by means of μSR was used [15]. The experimental data were analyzed using the MUSRFIT package [16].

Figure 1 shows the Fourier transform of TF-μSR time spectra reflecting the internal field distribution $P(B)$ in the $CaKFe_4As_4$ single-crystal sample. The results of field-cooled measurements in a field of $\mu_0 H_{ap} = 30$ mT [panel (a)] and 580 mT [panel (b)] above ($T = 42.2$ K) and below ($T = 1.55$ K) $T_c \simeq 35$ K are presented. The asymmetric $P(B)$ distributions at $T = 1.55$ K possess the basic features expected for an ordered vortex lattice, namely: The cutoff at low fields,

*rustem.khasanov@psi.ch

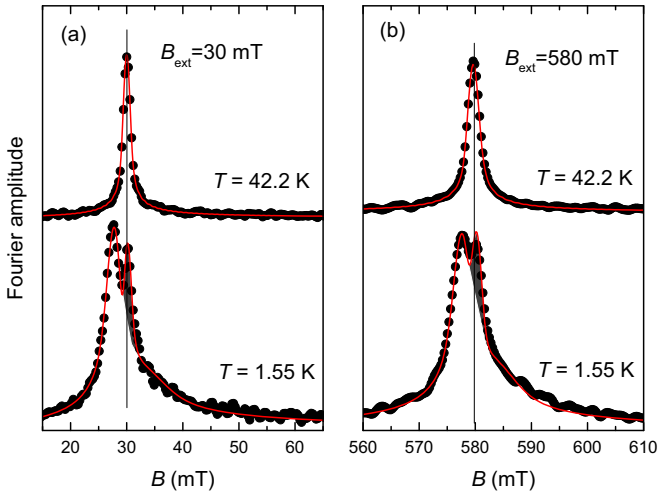

FIG. 1. Fourier transform of the TF-μSR time spectra obtained in an applied field of (a) $\mu_0 H_{ap} = 30$ mT and (b) $\mu_0 H_{ap} = 580$ mT above ($T = 42.2$ K) and below ($T = 1.55$ K) $T_c \simeq 35$ K. The red lines are the two- ($T = 42.2$ K) and three- ($T = 1.55$ K) component Gaussian fits corresponding to the field distribution $P(B)$ described by Eq. (1). The peak at $B = \mu_0 H_{ap}$ represents the background signal.

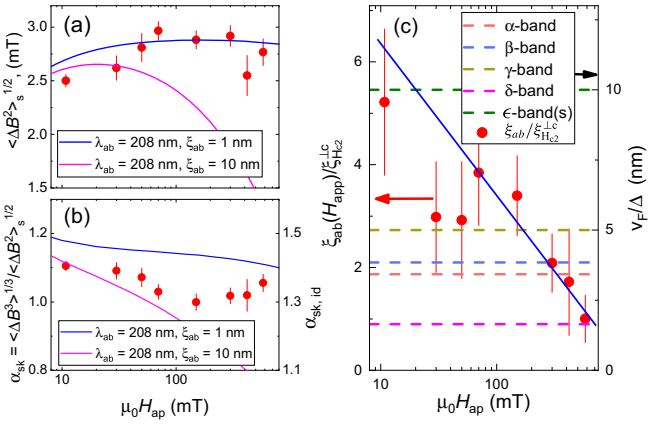

FIG. 2. (a) Field dependence of $\langle \Delta B^2 \rangle_s^{1/2}$ of $CaKFe_4As_4$ at $T = 1.55$ K. (b) Dependence of α_{sk} on H_{ap}. The pink and blue solid lines in (a) and (b) are calculations obtained within the framework of the London model with a Gaussian cutoff for $\lambda_{ab} = 208$, $\xi_{ab} = 10$ nm and $\lambda_{ab} = 208$, $\xi_{ab} = 1$ nm, respectively. (c) Dependence of $\xi_{ab}/\xi^{\perp c}_{Hc2}$ on H_{ap}. The dashed lines correspond to $\langle v_F \rangle_i / \Delta_{0,i}$ values ($i = \alpha$, β, γ, δ, or ϵ is the band index).

the peak shifted below H_{ap}, and the long tail towards the high-field direction (see, e.g., Refs. [15,17] and references therein). The sharp peak at $B = \mu_0 H_{ap}$ represents the residual background signal from muons missing the sample. The μSR time spectra were analyzed using a three-component Gaussian expression with the first (the temperature- and field-independent) component corresponding to the background contribution and another two components accounting for the asymmetric $P(B)$ distribution in the mixed state of the superconductor (see the Supplemental Material [18] and Refs. [24,25] for details). The time-domain expression is equivalent to a distribution in the field domain,

$$P(B) = P(B)_b + P(B)_s = \frac{\gamma_\mu A_b}{\sigma_b} \exp\left(-\frac{\gamma_\mu^2 (B - B_b)^2}{2\sigma_b^2}\right) + \sum_{i=1}^{2} \frac{\gamma_\mu A_i}{\sigma_i} \exp\left(-\frac{\gamma_\mu^2 (B - B_i)^2}{2\sigma_i^2}\right). \quad (1)$$

Indices b and s correspond to the background and the sample contributions, respectively. $A_b(A_i)$, $\sigma_b(\sigma_i)$, and $B_b(B_i)$ are the asymmetry, the relaxation rate, and the mean field of the background (ith sample) component. $\gamma_\mu = 2\pi \times 135.5342$ MHz/T is the muon gyromagnetic ratio. For $T \geqslant T_c$ the analysis of the sample contribution was simplified to a single Gaussian line shape.

The first moment ($\langle B \rangle$), the second- ($\langle \Delta B^2 \rangle$), and third-central moments ($\langle \Delta B^3 \rangle$) of $P(B)_s$ were obtained analytically (see the Supplemental Material [18]) and have the following physical interpretations: (i) The first moment (the mean field) is generally smaller than H_{ap} due to the diamagnetic nature of the superconducting state. The field shift $\mu_0 H_{ap} - \langle B \rangle$ scales with the sample magnetization [26]. (ii) The second moment encodes the broadening of the signal and contains contributions from the vortex lattice and the nuclear dipole field. The assumedly temperature-independent nuclear dipolar field contribution (σ_{nm}) is determined from measurements made above T_c. The superconducting component ($\langle \Delta B^2 \rangle_s$) is then obtained by subtracting σ_{nm} from the measured second moment: $\langle \Delta B^2 \rangle_s = \langle \Delta B^2 \rangle - \sigma_{nm}^2$. $\langle \Delta B^2 \rangle_s$ is a function of the magnetic penetration depth λ and the vortex core size $\xi \sim \xi_{Hc2}$ (ξ_{Hc2} is the coherence length as obtained from the upper critical field). In extreme type-II superconductors ($\lambda \gg \xi_{Hc2}$) and for fields much smaller than the upper critical field $\langle \Delta B^2 \rangle_s$ is proportional to λ^{-4} [27,28]. (iii) The third moment accounts for the asymmetric shape of $P(B)$, which is described via the skewness parameter $\alpha_{sk} = \langle \Delta B^3 \rangle^{1/3} / \langle \Delta B^2 \rangle_s^{1/2}$. In the limit of $\lambda \gg \xi$ and for realistic measurement conditions $\alpha_{sk} \simeq 1.2$ for a well-arranged triangular vortex lattice. It is very sensitive to structural changes in the vortex lattice which may occur as a function of temperature and/or magnetic field [29,30].

Figures 2(a) and 2(b) show the dependence of the square root of the second-moment $\langle \Delta B^2 \rangle_s^{1/2}$ and the skewness parameter α_{sk} on H_{ap} at $T = 1.55$ K. Since in our experiments the magnetic field was applied along the crystallographic c axis, both $\langle \Delta B^2 \rangle_s^{1/2}$ and α_{sk} are functions of the in-plane components of the magnetic penetration depth (λ_{ab}) and the vortex core size (ξ_{ab}). The experimental data were compared with calculations performed within the framework of the London model with a Gaussian cutoff for an ideal hexagonal vortex lattice (see the Supplemental Material part [18] and Refs. [27,31–33]).

The analysis reveals that both experimental $\langle \Delta B^2 \rangle_s^{1/2}$ and α_{sk} field dependencies can be described with an essentially field-independent $\lambda_{ab} \simeq 208$ nm and ξ_{ab} ranging from $\simeq 1$ to 10 nm. As an example, the solid curves in Figs. 2(a) and 2(b) correspond to the theory calculations for an ideal vortex lattice with $\lambda_{ab} = 208$, $\xi_{ab} = 10$ nm (the pink curve) and $\lambda_{ab} = 208$, $\xi_{ab} = 1$ nm (the blue curve). Note that due to vortex lattice distortions, which are always present in real

TABLE I. Parameters extracted and calculated from ARPES and μSR data. $\Delta_{0,i}$ is the zero-temperature value of the superconducting gap, $\langle v_F\rangle_i$ is the mean value of the Fermi velocity, $\langle d_F\rangle_i$ is the average diameter of the Fermi-surface sheet, and $\lambda_{ab,i}^{-2}(0)/\lambda_{ab}^{-2}(0)$ is the relative contribution of the ith band to $\lambda_{ab}^{-2}(0)$.

	$\Delta_{0,i}$ (meV)	$\langle v_F\rangle_i$ (eV nm)	$\langle d_F\rangle_i$ (nm^{-1})	$\frac{\lambda_{ab,i}^{-2}(0)}{\lambda_{ab}^{-2}(0)}$	Technique
α band	10.5(0.8)	0.036(1)	1.60(25)	0.073(11)	ARPES
β band	13.0(0.8)	0.050(2)	3.23(25)	0.202(15)	
γ band	8.0(0.6)	0.040(1)[a]	6.53(25)	0.323(12)	
δ band	12.0(1.3)	~0.008	3.30(25)	0.032(3)	
ϵ bands	2.4(2)	~0.025	~10.0[b]	0.370(40)	μSR

[a]Averaged over $h\nu = 6.7$- and 21.2-eV photon energies, Fig. 3.
[b]The sum of diameters.

superconducting samples, the experimentally observed α_{sk} is slightly smaller than the ideal value of $\alpha_{sk,id}$ obtained after calculations [17]. The independence of λ on the magnetic field is a characteristic feature of fully gapped superconductors. As shown by Kadono [34], λ increases with an increasing field if the superconducting gap contains nodes and is field independent if the gap is isotropic. Our results suggest, therefore, that $CaKFe_4As_4$ is a nodeless superconductor in good agreement with the previously reported data [8–10,12].

According to Fente *et al.* [10], the vortex core size in $CaKFe_4As_4$ *decreases* with an increasing field. Our experimental data are consistent with this finding. Figures 2(a) and 2(b) imply that the low-field $\langle B^2\rangle_s^{1/2}$ and α_{sk} points stay closer to the $\xi_{ab} = 10$ nm theory curves, whereas the high-field values are closer to $\xi_{ab} = 1$ nm curves. The field-induced decrease in ξ_{ab} also accounts for the local minimum on $\alpha_{sk}(H_{ap})$ at $\mu_0 H_{ap} \simeq 150$ mT [see Fig. 2(b)]. Under the assumption of field-independent $\lambda_{ab} = 208(4)$ and $\xi_{ab}(0.58\ \text{T}) = \xi_{H_{c2}}^{\perp c}$ ($\xi_{H_{c2}}^{\perp c} = 1.43$ nm is the coherence length as obtained from the upper critical field, Ref. [7]) the field dependence of $\xi_{ab}(H_{ap})/\xi_{H_{c2}}^{\perp c}$ was reconstructed {see Fig. 2(c) and the Supplemental Material for details [18]}.

The decrease in the vortex core size with an increasing field was observed in various conventional and unconventional superconductors in tunneling, magnetization and μSR experiments (see, e.g., Refs. [35–38]) as well as reported for $CaKFe_4As_4$ in tunneling experiments for fields exceeding 0.5 T [10]. The strongest effect was observed in multigap superconductors, such as MgB_2, $NbSe_2$ [36,39], and it was explained by the gap and Fermi-velocity-dependent length scales $\xi_i \propto \langle v_F\rangle_i/\Delta_{0,i}$ (i is the band index, and $\langle v_F\rangle$ is the mean value of the Fermi velocity). At low and high magnetic fields the vortex core size is governed by the high and low $\langle v_F\rangle_i/\Delta_{0,i}$ ratios, respectively. Previous ARPES experiments on $CaKFe_4As_4$ reveal the presence of at least four bands crossing the Fermi level with the corresponding Δ_0 values summarized in Table I [8]. Fermi velocities were further obtained in this Rapid Communication by performing linear fits of the band dispersion curves near the Fermi energy (see Fig. 3 and Table I). Obviously, the four bands reported in ARPES experiments do not explain the $\xi_{ab}/\xi_{H_{c2}}^{\perp c}$ vs H_{ap} behavior shown in Fig. 2(c).

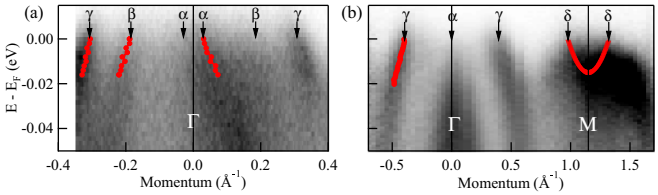

FIG. 3. Band dispersions of $CaKFe_4As_4$ at $T = 40$ K obtained in ARPES experiments: (a) by using the laser light source at the photon energy $h\nu = 6.7$ eV; (b) by using a plasma helium lamp with $h\nu = 21.2$ eV. The red lines are fits of the band dispersion curves near zero energy allowing to obtain the Fermi velocities. The units of momentum are kept in Å^{-1} for consistency with ARPES works.

One needs to assume the presence of an additional band or series of bands (ϵ bands) with $\langle v_F\rangle_\epsilon/\Delta_{0,\epsilon} \simeq 10$ nm. Bearing in mind that a small gap of $\Delta_{0,\epsilon} \simeq 2.4$ meV was obtained in our $\lambda_{ab}^{-2}(T)$ studies (see the following discussion) as well as reported in tunneling and superfluid density experiments by other groups [9,10,12], the average Fermi velocity within the ϵ bands is $\langle v_F\rangle_\epsilon \simeq 0.025$ eV nm. This value is well within the range for $\langle v_F\rangle$'s obtained by ARPES (see Table I).

Figure 4(a) compares the $\lambda_{ab}^{-2}(T)$ dependence obtained in the μSR experiment from the measured $\langle B^2\rangle^{1/2}$ at $\mu_0 H = 11$ mT (the red open circles) with the one calculated from the electronic band dispersion and the momentum-resolved superconducting gap measured by ARPES. Following Refs. [25,40–42], $\lambda_{ab}^{-2}(T)$ is determined as

$$\lambda_{ab}^{-2}(T) = \sum_i I_i \left[1 + 2\int_{\Delta_i(T)}^{\infty} \left(\frac{\partial f}{\partial E}\right) \frac{E\,dE}{\sqrt{E^2 - \Delta_i(T)^2}}\right]. \quad (2)$$

Here $f = [1 + \exp(E/k_BT)]^{-1}$ is the Fermi function, $\Delta_i(T) = \Delta_{0,i}\tanh\{1.82[1.018(T_c/T - 1)]^{0.51}\}$ [43], and I_i is the contribution of the ith gap to $\lambda_{ab}^{-2}(T = 0)$, which is

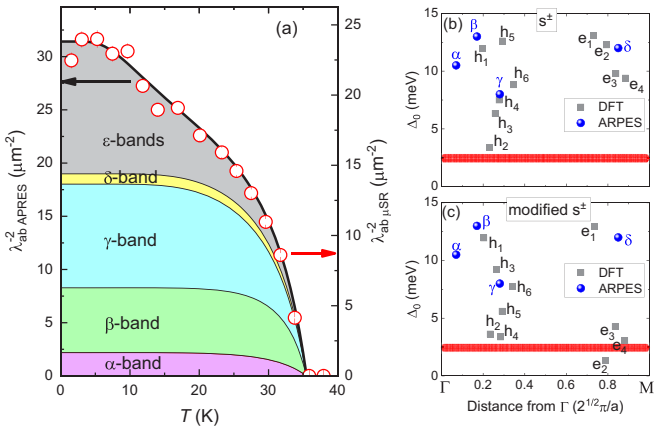

FIG. 4. (a) $\lambda_{ab}^{-2}(T)$ obtained from the measured $\langle B^2\rangle^{1/2}$ at $\mu_0 H = 11$ mT ($\lambda_{ab,\mu SR}^{-2}$) and inferred from ARPES data ($\lambda_{ab,ARPES}^{-2}$). The colored stripes are contributions of various Fermi surfaces to $\lambda_{ab}^{-2}(T)$. (b) Gaps as a function of momentum distance from Γ in hole (h) and electron (e) pockets as obtained from DFT calculations within the framework of the $s^{\pm}$ model [13]. (c) The same as in (b) but for a modified $s^{\pm}$ model. The red line is $\Delta_0 = 2.4$ meV. The blue points refer to the ARPES values [8].

obtained as [40]

$$I_i = \frac{e^2}{2\pi\varepsilon_0 c^2 h L_c} \oint_{i\text{th band}} v_{\mathrm{F},i}(\mathbf{k})dk. \quad (3)$$

Here e is the elementary charge, ε_0 is the electric constant, h is the Planck constant, c is the speed of light, L_c is the c-axis lattice parameter, and $\mathbf{k}$ is a momentum vector within the reciprocal space. Integrations are performed over the corresponding Fermi-surface contours.

The analysis reveals that the four bands observed in the ARPES experiment alone do not describe the experimentally measured $\lambda_{ab}^{-2}(T)$. In analogy with the above-discussed $\xi_{ab}(H_{\mathrm{ap}})$ results [see Fig. 2(c)] the presence of additional bands with smaller superconducting energy gaps are needed. The difference between the calculated and the measured λ_{ab}^{-2}'s allows access to the zero-temperature value of the superconducting gap of the ϵ bands. A reasonably good agreement is achieved for $\Delta_{0,\epsilon} \simeq 2.4(2)$ meV, $\lambda_{ab,\mathrm{ARPES}}(0) \simeq 187(11)$ nm, and a contribution to the zero-temperature superfluid density $[\lambda_{ab,\epsilon}^{-2}(0)/\lambda_{ab}^{-2}(0)]$ of $\simeq$37(4)% {see Fig. 4(a), Table I, and the Supplemental Material for details [18]}. With the known value of the Fermi velocity $\langle v_{\mathrm{F}}\rangle_\epsilon \simeq 0.025$ eV nm (see Table I), a sum of the diameters of additional bands $\langle d_{\mathrm{F}}\rangle_\epsilon \simeq 10.0\ \mathrm{nm}^{-1}$ was found. Two important points need to be mentioned. (i) The data in Fig. 4(a) were analyzed using only three independent parameters [$\Delta_{0,\epsilon}$, $\langle d_{\mathrm{F}}\rangle_\epsilon$, and $n = \lambda_{ab,\mathrm{ARPES}}(0)/\lambda_{ab,\mu\mathrm{SR}}(0)$]. The rest of the parameters were fixed to the values obtained in ARPES, magnetization, and $\xi_{ab}(H_{\mathrm{ap}})$ measurements [see Fig. 2(c), Ref. [7], and Table I]. (ii) The zero-temperature value of the in-plane penetration depth calculated from the ARPES data (including the contribution of the ϵ bands) results in $\lambda_{ab,\mathrm{ARPES}}(0) \simeq 187(11)$ nm, which is approximately 10% lower than 208(4) nm as determined by the μSR experiment. Note that a similar difference was reported for $Ba_{1-x}K_xFe_2As_2$ in Refs. [40,42].

Temperature dependencies of the superfluid density components of the α, β, γ, and δ bands follow the BCS type of mean-field behavior, whereas the response of ϵ bands is markedly different (see Fig. 3 in the Supplemental Material [18]). This may suggest that ϵ bands are only weakly involved in superconductivity and alone would have T_c on the order of 15 K only. Above 15 K the superconductivity in the ϵ bands remains due to the effects of interband coupling [44,45].

The $s^{\pm}$-gap symmetry with a sign change between hole and electron pockets in $CaKFe_4As_4$ was supported by the observation of the neutron-spin resonance peak with a characteristic energy of $\simeq$12.5 meV at the antiferromagnetic wave-vector $\mathbf{Q}_{\mathrm{AF}} = (\pi,\pi)$ [46,47]. We should emphasize, however, that the recent DFT calculations obtain two stable solutions for possible gap functions in $CaKFe_4As_4$. The first corresponds to the conventional $s^{\pm}$ state, whereas the second (modified $s^{\pm}$ state) allows an additional sign change within the hole and electron pockets with some gaps being small in magnitude [13]. The modified $s^{\pm}$ state enhances the spin response at the antiferromagnetic wave-vector (π,π) and, therefore, becomes consistent with the results of Iida *et al.* [46]. This enhancement, however, cannot be regarded as a pure spin resonance due to relatively small gap sizes on some electron and hole pocket bands. As a consequence, the resonance in $CaKFe_4As_4$ cannot be treated as a true spin excitation since its position is not *below* but *inside* the particle-hole continuum (see the Supplemental Material for details [18]).

Figures 4(b) and 4(c) show the superconducting gaps in hole (h) and electron (e) pockets as a function of momentum distance from the Γ point (the center of the Brillouin zone) as obtained from DFT calculations within the framework of the $s^{\pm}$ and modified $s^{\pm}$ models, respectively [13]. Within the $s^{\pm}$ approach only one out of ten bands has a gap value smaller than 5 meV [Fig. 4(b)]. Note that, due to the so-called red/blue shift reported by the authors of Ref. [13], one cannot rely on the band diameters obtained from the DFT calculations so the analysis similar to the one made above for obtaining $\lambda_{ab,\mathrm{ARPES}}^{-2}(T)$ cannot be performed. One would expect, however, that the contribution of nine bands to $\lambda_{ab}^{-2}(T)$ should be at least twice as high as for the four bands obtained in the ARPES experiments [see Fig. 4(a)]. This would lead to complete disagreement between the calculated and the experimentally measured $\lambda_{ab}^{-2}(T)$ dependencies. In contrast, within the modified $s^{\pm}$ model 5 (two holes and three electron) bands have gap values close to $\Delta_0 = 2.4$ meV [Fig. 4(c)]. They may account, therefore, for a 37% contribution to $\lambda_{ab}^{-2}(0)$ (see Table I). The other five bands left (four hole and one electron band) result in gap values comparable with that obtained in the ARPES experiments. This implies that the modified $s^{\pm}$ model agrees better with our experimental findings.

To conclude, the temperature and the magnetic-field dependencies of the in-plane magnetic penetration depth λ_{ab} and the field dependence of the vortex core size ξ_{ab} in the $CaKFe_4As_4$ single crystal were studied by means of muon-spin rotation. A comparison of the temperature dependence of λ_{ab}^{-2} measured by μSR to the one determined from the ARPES experiments confirms the presence of multiple gaps at the Fermi level. An agreement between the μSR and the ARPES data requires the presence of additional bands which are characterized by small superconducting gaps with an averaged zero-temperature value of $\Delta_0 = 2.4(2)$ meV. Our data suggest that the order parameter in $CaKFe_4As_4$ may acquire a more complex form than the simple $s^{\pm}$ symmetry. The gap sign change occurs not just between the electron and hole pockets, but also within pockets of similar types. Such a gap state is favored by weakened interband repulsion and yields further interesting consequences for the spin resonance.

The work was performed at the Swiss Muon Source (SμS), Paul Scherrer Institut (PSI, Switzerland). R.K. acknowledges D. V. Evtushinsky for helpful discussions and J. Barker for help with the Rapid Communication preparation. W.R.M. was supported by the Gordon and Betty Moore Foundation's EPiQS Initiative through Grant No. GBMF4411. I.E. acknowledges support from the project of the state assignment of KFU in the sphere of scientific activities, Grant No. 3.2166.2017/4.6 Work at Ames Laboratory was supported by the US Department of Energy, Office of Basic Energy Sciences, Division of Materials Sciences and Engineering. Ames Laboratory is operated for the US Department of Energy by Iowa State University under Contract No. DE-AC02-07CH11358.

[1] Y. Kamihara, T. Watanabe, M. Hirano, and H. Hosono, J. Am. Chem. Soc. **130**, 3296 (2008).

[2] F.-C. Hsu, J.-Y. Luo, K.-W. Yeh, T.-K. Chen, T.-W. Huang, P. M. Wu, Y.-C. Lee, Y.-L. Huang, Y.-Y. Chu, D.-C. Yan, and M.-K. Wu, Proc. Natl. Acad. Sci. U.S.A. **105**, 14262 (2008).

[3] G. R. Stewart, Rev. Mod. Phys. **83**, 1589 (2011).

[4] X. Chen, P. Dai, D. Feng, T. Xiang, and F. C. Zhang, Nat. Sci. Rev. **1**, 371 (2014).

[5] J. Paglione and R. L. Greene, Nat. Phys. **6**, 645 (2010).

[6] A. Iyo, K. Kawashima, T. Kinjo, T. Nishio, S. Ishida, H. Fujihisa, Y. Gotoh, K. Kihou, H. Eisaki, and Y. Yoshida, J. Am. Chem. Soc. **138**, 3410 (2016).

[7] W. R. Meier, T. Kong, U. S. Kaluarachchi, V. Taufour, N. H. Jo, G. Drachuck, A. E. Böhmer, S. M. Saunders, A. Sapkota, A. Kreyssig, M. A. Tanatar, R. Prozorov, A. I. Goldman, F. F. Balakirev, A. Gurevich, S. L. Bud'ko, and P. C. Canfield, Phys. Rev. B **94**, 064501 (2016).

[8] D. Mou, T. Kong, W. R. Meier, F. Lochner, L.-L. Wang, Q. Lin, Y. Wu, S. L. Bud'ko, I. Eremin, D. D. Johnson, P. C. Canfield, and A. Kaminski, Phys. Rev. Lett. **117**, 277001 (2016).

[9] K. Cho, A. Fente, S. Teknowijoyo, M. A. Tanatar, K. R. Joshi, N. M. Nusran, T. Kong, W. R. Meier, U. Kaluarachchi, I. Guillamón, H. Suderow, S. L. Bud'ko, P. C. Canfield, and R. Prozorov, Phys. Rev. B **95**, 100502(R) (2017).

[10] A. Fente, W. R. Meier, T. Kong, V. G. Kogan, S. L. Bud'ko, P. C. Canfield, I. Guillamon, and H. Suderow, Phys. Rev. B **97**, 134501 (2018).

[11] J. Cui, Q.-P. Ding, W. R. Meier, A. E. Böhmer, T. Kong, V. Borisov, Y. Lee, S. L. Bud'ko, R. Valenti, P. C. Canfield, and Y. Furukawa, Phys. Rev. B **96**, 104512 (2017).

[12] P. K. Biswas, A. Iyo, Y. Yoshida, H. Eisaki, K. Kawashima, and A. D. Hillier, Phys. Rev. B **95**, 140505(R) (2017).

[13] F. Lochner, F. Ahn, T. Hickel, and I. Eremin, Phys. Rev. B **96**, 094521 (2017).

[14] A. Amato, H. Luetkens, K. Sedlak, A. Stoykov, R. Scheuermann, M. Elender, A. Raselli, and D. Graf, Rev. Sci. Instrum. **88**, 093301 (2017).

[15] R. Khasanov, H. Zhou, A. Amato, Z. Guguchia, E. Morenzoni, X. Dong, G. Zhang, and Z.-X. Zhao, Phys. Rev. B **93**, 224512 (2016).

[16] A. Suter and B. M. Wojek, Phys. Procedia **30**, 69 (2012).

[17] A. Maisuradze, R. Khasanov, A. Shengelaya, and H. Keller, J. Phys.: Condens. Matter **21**, 075701 (2009).

[18] See Supplemental Material at http://link.aps.org/supplemental/10.1103/PhysRevB.97.140503 for a description of the experimental techniques and the data analysis procedure, which includes Refs. [19–23].

[19] R. Jiang, D. Mou, Y. Wu, L. Huang, C. D. McMillen, J. Kolis, H. G. Giesber, J. J. Egan, and A. Kaminski, Rev. Sci. Instrum. **85**, 033902 (2014).

[20] R. Khasanov, D. G. Eshchenko, D. Di Castro, A. Shengelaya, F. La Mattina, A. Maisuradze, C. Baines, H. Luetkens, J. Karpinski, S. M. Kazakov, and H. Keller, Phys. Rev. B **72**, 104504 (2005).

[21] T. M. Riseman, J. H. Brewer, K. H. Chow, W. N. Hardy, R. F. Kiefl, S. R. Kreitzman, R. Liang, W. A. MacFarlane, P. Mendels, G. D. Morris, J. Rammer, J. W. Schneider, C. Niedermayer, and S. L. Lee, Phys. Rev. B **52**, 10569 (1995).

[22] F. Ahn, I. Eremin, J. Knolle, V. B. Zabolotnyy, S. V. Borisenko, B. Büchner, and A. V. Chubukov, Phys. Rev. B **89**, 144513 (2014).

[23] N. Qureshi, P. Steffens, D. Lamago, Y. Sidis, O. Sobolev, R. A. Ewings, L. Harnagea, S. Wurmehl, B. Büchner, and M. Braden, Phys. Rev. B **90**, 144503 (2014).

[24] R. Khasanov, I. L. Landau, C. Baines, F. La Mattina, A. Maisuradze, K. Togano, and H. Keller, Phys. Rev. B **73**, 214528 (2006).

[25] R. Khasanov, A. Shengelaya, A. Maisuradze, F. La Mattina, A. Bussmann-Holder, H. Keller, and K. A. Müller, Phys. Rev. Lett. **98**, 057007 (2007).

[26] M. Weber, A. Amato, F. N. Gygax, A. Schenck, H. Maletta, V. N. Duginov, V. G. Grebinnik, A. B. Lazarev, V. G. Olshevsky, V. Yu. Pomjakushin, S. N. Shilov, V. A. Zhukov, B. F. Kirillov, A. V. Pirogov, A. N. Ponomarev, V. G. Storchak, S. Kapusta, and J. Bock, Phys. Rev. B **48**, 13022 (1993).

[27] E. H. Brandt, Phys. Rev. B **37**, 2349(R) (1988).

[28] E. H. Brandt, Phys. Rev. B **68**, 054506 (2003).

[29] S. L. Lee, P. Zimmermann, H. Keller, M. Warden, I. M. Savić, R. Schauwecker, D. Zech, R. Cubitt, E. M. Forgan, P. H. Kes, T. W. Li, A. A. Menovsky, and Z. Tarnawski, Phys. Rev. Lett. **71**, 3862 (1993).

[30] C. M. Aegerter, J. Hofer, I. M. Savić, H. Keller, S. L. Lee, C. Ager, S. H. Lloyd, and E. M. Forgan, Phys. Rev. B **57**, 1253 (1998).

[31] E. H. Brandt, J. Low Temp. Phys. **26**, 709 (1977).

[32] E. H. Brandt, J. Low Temp. Phys. **73**, 355 (1988).

[33] J. Rammer, Physica C **177**, 421 (1991).

[34] R. Kadono, J. Phys.: Condens. Matter **16**, S4421 (2004).

[35] J. E. Sonier, J. H. Brewer, and R. F. Kiefl, Rev. Mod. Phys. **72**, 769 (2000).

[36] J. E. Sonier, J. Phys.: Condens. Matter **16**, S4499 (2004).

[37] V. G. Kogan, R. Prozorov, S. L. Bud'ko, P. C. Canfield, J. R. Thompson, J. Karpinski, N. D. Zhigadlo, and P. Miranović, Phys. Rev. B **74**, 184521 (2006).

[38] A. Fente, E. Herrera, I. Guillamon, H. Suderow, S. Manas-Valero, M. Galbiati, E. Coronado, and V. G. Kogan, Phys. Rev. B **94**, 014517 (2016).

[39] M. R. Eskildsen, M. Kugler, S. Tanaka, J. Jun, S. M. Kazakov, J. Karpinski, and Ø. Fischer, Phys. Rev. Lett. **89**, 187003 (2002).

[40] D. V. Evtushinsky, D. S. Inosov, V. B. Zabolotnyy, M. S. Viazovska, R. Khasanov, A. Amato, H.-H. Klauss, H. Luetkens, C. Niedermayer, G. L. Sun, V. Hinkov, C. T. Lin, A. Varykhalov, A. Koitzsch, M. Knupfer, B. Büchner, A. A. Kordyuk, and S. V. Borisenko, New J. Phys. **11**, 055069 (2009).

[41] M. Tinkham, *Introduction to Superconductivity* (Krieger, Malabar, FL, 1975).

[42] R. Khasanov, D. V. Evtushinsky, A. Amato, H.-H. Klauss, H. Luetkens, C. Niedermayer, B. Büchner, G. L. Sun, C. T. Lin, J. T. Park, D. S. Inosov, and V. Hinkov, Phys. Rev. Lett. **102**, 187005 (2009).

[43] A. Carrington and F. Manzano, Physica C **385**, 205 (2003).

[44] H. Suhl, B. T. Matthias, and L. R. Walker, Phys. Rev. Lett. **3**, 552 (1959).

[45] V. A. Moskalenko, Phys. Met. Metallogr. (USSR) **8**, 25 (1959).

[46] K. Iida, M. Ishikado, Y. Nagai, H. Yoshida, A. D. Christianson, N. Murai, K. Kawashima, Y. Yoshida, H. Eisaki, and A. Iyo, J. Phys. Soc. Jpn. **86**, 093703 (2017).

[47] $\mathbf{Q}_{\mathrm{AF}} = (\pi,\pi)$ corresponds to the $CaKFe_4As_4$ Brillouin zone. It is typically equal to $(\pi,0)$ for most Fe-SCs.